Slow-Time Changes in Human EMG Muscle Fatigue States Are Fully Represented in Movement Kinematics

Miao Song[1], David B. Segala[1], Jonathan B. Dingwell[2], and David Chelidze[1,*]
[1]Nonlinear Dynamics Laboratory, Mechanical Engineering & Applied Mechanics
University of Rhode Island, Kingston, RI 02881
[2]Nonlinear Biodynamics Laboratory, Kinesiology & Health Education
University of Texas at Austin, Austin, TX 78712

Accepted for publication on 28 August, 2008 by the *Biomechanical Engineering*

Abstract

The ability to identify physiologic fatigue and related changes in kinematics can provide important tool for diagnosing fatigue related injuries. This study examined an exhaustive cycling task to demonstrate how changes in movement kinematics and variability reflect underlying changes in local muscle states. Motion kinematics data were used to construct fatigue features. Their multivariate analysis, based on *smooth orthogonal decomposition*, was used to reconstruct physiological fatigue. Two different features composed of: (1) *standard statistical metrics* (SSM), which were a collection of standard *long-time* measures, and (2) *phase space warping* (PSW) based metrics, which characterized *short-time* variations in the phase space trajectories were considered. Movement kinematics and surface electromyography (EMG) signals were measured from the lower extremities of seven highly trained cyclists as they cycled to voluntary exhaustion on a stationary bicycle. Mean and median frequencies from the EMG time series were computed to measure the *local* fatigue dynamics of individual muscles, *independent* of the SSM- and PSW-based features, which were extracted *solely* from the kinematic data. Nonlinear analysis of kinematic features was shown to be essential for capturing full multidimensional fatigue dynamics. A four-dimensional fatigue manifold identified using nonlinear PSW-based analysis of kinematic data was shown to adequately predict all EMG-based individual muscle fatigue trends. While SSM-based analyses showed similar dominant *global* fatigue trends, they failed to capture individual muscle activity in a low dimensional manifold. Therefore, nonlinear PSW-based analysis of strictly kinematic time series data directly predicted all of the local muscle fatigue trends in a low-dimensional systemic fatigue trajectory. These results provide the first direct quantitative link between changes in muscle fatigue dynamics and resulting changes in movement kinematics.

1 Introduction

As people perform repetitive movements over extended periods of time, they develop muscle fatigue, defined as a decrease in the force-generating output of a muscle after repeated use [1]. When muscles fatigue, people compensate by changing their movement biomechanics to limit the use of the specific fatigued muscle(s) [2, 3, 4, 5, 6, 7]. It has been hypothesized that continuing deterioration of a fatigued muscle, or changes in biomechanics that lead to sub-optimal movement patterns and possibly to mal-adaptive joint loading, can increase the risks of serious injury, including repetitive strain injuries [8, 9]. Alternatively, it is possible that continuing with the same movement pattern could in some cases lead to more repetitive strain injuries than shifting patterns. Increased popularization of both recreational and competitive cycling [10] has led to an increase in cycling-related repetitive strain injuries. Knee pain is the most common repetitive strain injury

*Corresponding author. Email: chelidze@egr.uri.edu. Phone/fax: 401-874-2356/55. http://www.mce.uri.edu/chelidze/

associated with cycling [10, 11, 12]. Between 42–65% of recreational cyclists may experience overuse knee pain [13, 14]. The prevalence of all non-traumatic injuries among cyclists may be as high as 85% [15]. Many of these injuries may result from biomechanical alterations associated with muscle fatigue.

The development of acute fatigue in cycling is a complex process involving energetic, cardiovascular, neuromuscular, biomechanical, and psychological factors [16, 17]. While several studies have measured fatigue-related changes in performance related to mechanical and cardiovascular output, biomechanical factors like muscle activity and joint kinematics have been less studied. While very short (5–30 sec.) bouts of maximal effort cycling altered the torque produced by trained cyclists [10, 11, 12], links to changes in muscle activity or joint kinematics were not assessed. Moderate duration bouts (5–10 min.) of exhaustive cycling caused declines in cardiac output, muscle blood flow, and oxygen uptake and delivery [18, 19]. However, changes in muscle activity or kinematics were not assessed. Long bouts (1–5 hrs.) of sub-maximal cycling altered both neuromuscular central drive and peripheral muscular fatigue mechanisms [20, 21, 22]. However, these authors did not examine how these physiological changes affected cycling kinematics. Optimization studies predict how muscle activations produce biomechanical movement patterns during non-fatigued cycling [23, 24], but have not examined how fatigue affects cycling biomechanics. One study recently showed that both movement kinematics and muscle fatigue states fluctuate non-monotonically over time as highly-trained subjects fatigued during a maximal cycling task [25]. Changes in muscle fatigue state generally preceded specific changes in movement kinematics, thus establishing a direct link between changes in muscle fatigue state and subsequent changes in movement kinematics during cycling. However, the analyses used in that study were not designed to directly track and/or predict each cyclist's level of fatigue directly from the changes observed in their pedaling kinematics.

The ability to identify early fatigue-related changes in easily recordable biomechanical measures could provide an important tool for early diagnosis and/or prevention of repetitive strain injuries. To acquire this ability, one needs to understand local individual muscle fatigue progression, as well as global (overall organism) physiologic fatigue dynamics. This includes the understanding of the coupling between these fatigue processes and biomechanics. There are two possible ways to acquire this information: (1) first-principles, physics-based modeling and (2) phenomenological understanding based on experimental data analysis. The former is complicated by the complexity of the systems involved in physiologic fatigue processes; and even if successful, would still need to be confirmed by the latter. In this paper, we establish basic experimental evidence from multivariate analysis of kinematic data that can be used to guide the development of, or confirm the validity of, theoretical fatigue models.

Surface *electromyography* (EMG) has been used extensively to quantify changes in muscle function during fatigue [26]. In general, when a muscle becomes fatigued, the bandwidth of the EMG power spectrum compresses towards lower frequencies [26, 27]. In particular, the EMG of fatigued muscle exhibits a decrease in the mean and/or median frequency of the power spectrum, due at least in part to decreases in motor unit firing rates, recruitment of additional slower motor units, and/or a reduction in muscle fiber action potential conduction velocity, among other factors [26]. Thus, muscle fatigue can be identified by the decrease of the EMG center frequency. While the underlying causes of these shifts are still in debate, the phenomenon itself is highly robust, especially for sustained isometric contractions [26]. Additionally, "short-time" Fourier transform methods have been developed [28] and subsequently validated [29, 30] that can accurately track slowly varying changes in muscle fatigue across multiple dynamic contractions. To date, only one study has attempted to correlate changes in EMG central frequencies with changes in coordination [25] and no studies have attempted to directly *track* changes in muscle fatigue state over time as fatigue sets in from kinematic data.

In the engineering field of structural health monitoring, many practical methods of damage identification have been developed [31], where a structural response is related to the underlying damage process. The physics community has also investigated nonstationary systems with drifting parameters. Some of these methods are independent of underlying nonstationarity or damage physics and use readily measurable time series for the analysis. Physiologic fatigue accumulation is in several ways similar to these problems, where nonstationarity/damage (fatigue) accumulates slowly over time in the system characterized by faster dynamics (motion). In this paper, methods used for identifying damage/nonstationarity-causing processes in dynamical systems were applied to analyze human movement kinematics data. The purpose of the present

study was to demonstrate that the fatigue information obtainable from standard EMG-based estimates was also independently present in the kinematic data. Furthermore, we wanted to determine if the kinematics-based analysis could be used to reconstruct the corresponding fatigue phase space trajectory, as well as individual (local) muscle fatigue trends described by conventional EMG analysis.

Two philosophically different methods methods of characterizing the system dynamics were explored in this study: (1) a multivariate modification of the *standard statistical metrics* (SSM) based dynamical system's parameter space reconstruction proposed in Ref. [32], and (2) the *phased space warping* (PSW) based damage identification method described in Ref. [33, 34]. Both methods were chosen for their ability to reconstruct the dynamics of hidden slow processes using fast-time measurements. However, SSM uses an *arbitrary* (i.e., based on a heuristic "best guess" approach) collection of *long-time* standard metrics (i.e., statistical averages computed over relatively long time windows) to identify underlying slowly evolving processes. Conversely, PSW computes a *short-time* metric that is *specifically* derived based on fundamental dynamical principles. By using *short-time* metrics, the PSW method can better detect the desired slow time scale drift even in the presence of rather rapid changes in the fast time scale dynamics, which do occur in cycling [25]. The performance and versatility of these two approaches in tracking physiologic fatigue was evaluated and contrasted. Specifically, this study tested the hypotheses (1) that contemporary dynamical systems based multivariate analyses of kinematic data would capture both the global and local muscle fatigue dynamics and (2) that generically, PSW-based features would be superior to SSM-based features in tracking physiologic fatigue.

The study presented here is a natural extension of the work described in [35], where a scalar version of PSW-based damage identification was used to track slowly varying changes in the treadmill inclination angle as five healthy adults walked on a motorized treadmill at their preferred speed. In Ref. [35], it was shown that PSW-based damage identification methods could successfully track an externally imposed slow-time scale *mechanical* process (i.e., increasing treadmill inclination angle) from the independently recorded human walking kinematics. The present study extends that work in three specific ways. First, this study examined a different task (i.e., *cycling*) to demonstrate that the previous results were not specific to the task being performed. Second, the present study tracked a slowly evolving *physiological* process (i.e., muscle fatigue), rather than a strictly *mechanical* process. Finally, the present study used *vector-valued* metrics, rather than *scalar* metrics, since physiologic fatigue was expected to be a more complex, multidimensional/multiscale process.

2 Fatigue Identification Methodology

As in [33, 34, 35], muscle fatigue was viewed as evolving in a hierarchical dynamical system:

$$\dot{x} = f(x, \mu(\phi), t)\,, \quad \dot{\phi} = \varepsilon g(\phi, x)\,, \quad \text{and} \quad y = h(x)\,, \tag{1}$$

where overdot denoted time rate-of-change; x was a fast-time dynamic variable describing movement kinematics; ϕ was a slow-time variable describing muscle fatigue dynamics, which altered a parameter vector μ in the fast-time system; t was time; and ε was a small rate constant describing time scale separation. It was assumed that the fast-time dynamics can be measured through some scalar measurement function h generating scalar time series y. The objective was then to use these measured time series to identify or reconstruct the slow-time evolution of the fatigue variable ϕ. In what follows, the movement kinematics measurements were used as fast-time series. In addition, independent of kinematic analysis, standard EMG-based statistics, i.e. mean and median frequency, were used as measures of local individual muscle fatigue dynamics for comparison purposes.

The fatigue identification framework had two distinct stages: (1) selection and estimation of feature vectors from fast-time time series at different stages of fatigue accumulation, and (2) multivariate analysis of features to identify slow-time manifold of fatigue dynamics. The slow-time feature vectors were evaluated over the time windows corresponding to an intermediate time scale, defined as a time scale over which the variations in the fatigue variables are negligible.

2.1 Feature Vector Construction

2.1.1 Long-Time SSM-Based Features

The approach we adopted here was based on Güttler et al. [32], where smooth parameter variations in the equations of motion of dynamical systems were identified by time series analysis. In particular, time series data were used to construct feature vectors by calculating some standard or common *long-time* statistical measures. The selection of particular statistical measures was arbitrary. However, if a large enough set of *appropriate* measures is considered, the feature space should provide an embedding for the smoothly varying parameters. The main drawback identified in the method is that singularities due to the bifurcations[1] in deterministic dynamical system caused discontinuities in the embedding. These discontinuities were claimed to disappear for slightly noisy systems. However, other studies [36, 34] show that these bifurcations can still cause discontinuities for real dynamical systems. Other methods for reconstructing drifting parameters [37, 38] assumed there was only one scalar parameter variation. Therefore, they cannot be used for our purposes, where multidimensional parameter variation is expected.

In the SSM-based method, feature vectors were composed of both linear and nonlinear *long-time* measures (i.e., statistical measures that are defined for infinite time, or as time approaches infinity). These statistics are obviously estimated using finite length time series, but usually require a large number of sample points for accurate results. The choice of these metrics is somewhat arbitrary. While some metrics might work well for one application, different metrics might work better for another. Unfortunately, there is no systematic way to determine the optimal choice of metrics *a priori*.

In this study, a generic set of metrics was calculated from time series $\{y_i\}_{i=1}^N$ recorded during any given time window $\{j\}_{j=1}^M$, where N is the total number of point in each time window, and M is the total number of time windows. The linear part of the *feature vectors* $\{e^j\}_{j=1}^M$ was composed of the estimated mean $\bar{y} = \langle y \rangle \approx \frac{1}{N}\sum_{i=1}^N y_i$, variance $\sigma^2 = \langle (y-\bar{y})^2 \rangle \approx \frac{1}{N}\sum_{i=1}^N (y_i - \bar{y})^2$, and several points from power spectral density $S_{yy}(\omega)$ [39], that exhibited large variations over the slow-time scale. The nonlinear part of the feature vector e^j was composed of skewness $\gamma_3 = \langle (y-\bar{y})^3 \rangle / (\sigma^2)^{3/2}$, kurtosis [40] $\gamma_4 = \langle (y-\bar{y})^4 \rangle / (\sigma^2)^2$, *Katz-Servick fractal dimension*[2] [42], and correlation sum[3] $C(\epsilon)$ [39]. Please note that this choice of metrics might not be optimal, but it served the purpose of this paper. The arbitrariness of the selected metrics and the need for further extensive analysis to determine some "optimal" set of metrics for a particular application is one of the drawbacks of this method.

In [32], an arbitrary collection of measures (e.g., polynomial model coefficients, mean, standard deviation, and maximal Lyapunov exponent) was used to show the embedding of the parameter variations. It was not discussed how these measures were selected. In this paper, we use a new multivariate analysis of the features to identify the optimal embedding space (i.e., linear subspace of the feature space) for a given fatigue dynamics. The details of this analysis are exactly the same for both SSM and PSW-based features and are given in Sec. 2.2.

2.1.2 Short-Time PSW-Based Features

The PSW method was part of the dynamical systems approach to damage identification [34, 33]. Here the feature vectors were constructed by calculating PSW-based *short-time* statistics in the reconstructed phase space using measured time series [43]. In this case, the choice of the metrics *was not* arbitrary, since there was a strong *a priori* rationale for the selection of the metric. Due to this particular choice, the short-time measures were smooth functions of drifting variables even during bifurcations. Thus, the PSW-based

[1] Generic definition of bifurcation is a sudden appearance of a qualitatively different solution for a nonlinear system as some parameter is varied. In our case slowly accumulating fatigue acts as slowly varying parameter in a nonlinear system describing the movement kinematics. Overall, the changes in movement patterns are expected to be slowly varying, but could also be rather sudden as fatigue accumulates. These changes might not conform to true definition of bifurcations, however, long-time average statistics are still expected to vary discontinuously with any such sudden change in kinematics.

[2] Here, Katz-Servick fractal dimension, which indicates how completely a fractal fills a space [41], was used for simplicity of calculation. Focus here was on a measure that reflected the fractality of data, not an accurate estimates of fractal dimension.

[3] $C(\epsilon)$ reflects the probability that two points in phase space are within ϵ distance.

analyses were expected to be insensitive to any sudden changes in cycling kinematics, whereas the SSM-based analyses were not. The approach used here was described in detail elsewhere [34, 33], and has been successfully applied to different types of electromechanical systems all with different mechanisms of slow-time drifts [36, 43, 44].

Given a time series recorded over some intermediate time window, $\{y_i\}_{i=1}^{N}$, the corresponding phase space was reconstructed using *delay coordinate embedding* [45]. In particular, a d-dimensional vector time-series $\{y(i)\}_{i=1+(d-1)\tau}^{N}$ was generated as:

$$y(i) = [y_i, y_{i-\tau}, \ldots, y_{i-(d-1)\tau}]^T \,, \tag{2}$$

where superscript T indicates matrix transpose, *embedding dimension* d and *delay time* τ were estimated using false nearest neighbors and average mutual information methods described in detail in Ref. [39]. The embedded points in this space were governed by an as yet undetermined map of the form:

$$y(i+1) = P(y(i); \phi) \,, \tag{3}$$

where generally nonlinear map P was expected to change as fatigue variable ϕ slowly drifts.

The basic idea of PSW-based metrics was to characterize deformation of the phase space trajectory by looking at the single-time-step reference model prediction error,

$$\begin{aligned} e_R(y(i); \phi) \equiv e_R(y(i)|_\phi; \phi) &\equiv y(i+1)|_\phi - y(i+1)|_{\phi_R} \\ &= y(i+1) - P(y(i); \phi_R) \,, \end{aligned} \tag{4}$$

where ϕ was the current muscle fatigue state, ϕ_R was the reference or unfatigued state, and $(\cdot)|_\phi$ indicated $(\cdot)$ calculated for the particular ϕ value. In addition, $y(i+1)|_\phi$ did not need to be estimated, since both $y(i)|_\phi$ and $y(i+1)|_\phi$, were reconstructed from the current window of measured time series. However, the reference reconstructed phase space does not have a particular point $y|_{\phi_R}$ matching exactly $y(i)|_\phi$. Therefore, the reference window of time series was used to develop a predictive model $P(y(i); \phi_R)$ and to estimate $y(i+1)|_{\phi_R}$.

Irrespective of the type of model used for the estimation of the reference model prediction error, it was expected to vary from point to point as a function of local trajectory curvature. In addition, the accuracy of the model was expected to be a function of the local probability density of the reference phase space points. Thus, some regions of the phase space have better models and/or more accurate estimates of the single-time-step reference model prediction error. To average out modeling errors and develop robust features, the reference phase space was partitioned into N_e disjoint hyper-cuboids $\{\mathcal{B}_i\}_{i=1}^{N_e}$ that contained approximately the same number of reference points, and the expected value of $\|e_R(y; \phi)\|$ was evaluated in each of them:

$$e_i(\phi) = \frac{1}{N_i} \sum_{y \in \mathcal{B}_i} \|e_R(y; \phi)\| \,, \tag{5}$$

where, N_i was the number of points in $\mathcal{B}_i$. Then, for each time window j, all these averaged errors were assembled into an N_e-dimensional feature vector as:

$$e^j = [e_1(\phi), e_2(\phi), \ldots, e_{N_e}(\phi)] \,. \tag{6}$$

Linear Model Based Features

Assuming that measured time series originated from linear fast-time processes, *autoregressive moving average* models were used to describe them. The linear prediction model assumes each output sample of a signal, y_i, is a linear combination of the past p outputs (that is, it can be "linearly predicted" from these outputs), and that the coefficients are constant from sample to sample:

$$y_{i+1}|_{\phi_R} = P(y(i); \phi_R) = a_1 y_i + a_2 y_{i-1} + ... + a_p y_{i-p+1} = a y(i) \,, \tag{7}$$

where $p = d$ is the order of the prediction model, which is the same as embedding dimension; $\tau = 1$; and $a = [a_1, \ldots, a_p]$. Here, the model P was scalar, since $y(i+1)$ will have only y_{i+1} coordinate that is uniquely

new when compared to $y(i)$ due to $\tau = 1$. Once the model was built, the scalar single-time-step reference model prediction error was estimated as:

$$e_R(y_i; \phi) = y_{i+1} - y_{i+1}|_{\phi_R}\,, \tag{8}$$

where $y_{i+1} = y_{i+1}|_{\phi}$ was the point (sample) in the current window of the time series and $y_{i+1}|_{\phi_R}$ was the predicted image for the reference window of the time series, as described by Eq. (7). Using one part of the reference time series to train the model, and another part to validate the model, an optimized order of linear model was obtained by minimizing prediction error in the least-squares sense.

For the linear model based features, three middle coordinates (indexes $m - l$, m, and $m + l$) of the feature vector e^j were selected for phase space partitioning. Here $m = \text{round}(p/2)$ and the choice of l was somewhat arbitrary and did not alter results in a noticeable way. Each of these coordinates was used in sequence to section data into subspaces containing approximately the same number of points. If the number of divisions along each of these coordinates is m_1, m_2, and m_3, then $N_e = m_1 m_2 m_3$.

Nonlinear Model Based Features

Following the methodological approach outlined in [34, 33, 35], local linear models were used to model $P(y(i); \phi_R)$ in Eq. (3):

$$y(i+1)|_{\phi_R} = P(y(i); \phi_R) \approx A_i y(i) + b_i\,, \tag{9}$$

where the model parameter matrix A_i and a parameter vector b_i were determined for each point $y(i)$ separately [36]. In particular, 16 nearest neighbors of $y(i)$ and their images one time step later in the reference reconstructed phase space were used to find the local model parameters in the least-squares sense.

For the nonlinear model based features, the phase space partitioning was done using equiprobable *kd*-tree based partitioning of the reconstructed reference phase space points. As a result, the phase space was partitioned into N_e disjoint hyper-cuboids containing approximately the same number of points.

2.2 Smooth Orthogonal Decomposition

The feature vectors described in previous section were evaluated in each of the consequent time windows, and were row-wise concatenated in time sequence into a tracking matrix Y for further analysis. If there were a total of M windows in the time series, then $Y \in \mathbb{R}^{M \times N_e}$, where N_e was the dimension of the features used. Güttler et al. [32] claimed that parameter variations were embedded into this feature space if N_e was high enough. However, their work focused on (almost) noise free numerical models with unlimited amounts of data available for feature estimation. In realistic practical situations, one deals with limited amounts of data that are noisy. Furthermore, the features are also contaminated with bifurcation noise [36, 34, 33] that causes discontinuities in long-time SSM-based features and changes in the probability distributions in the reconstructed phase space for short-time PSW-based features. To deal with all of these variabilities, a multivariate analysis based on *smooth orthogonal decomposition* [46] was conducted.

The original idea of smooth orthogonal decomposition was developed for extracting a smooth, deterministic trend from damage tracking metrics [47]. It was later extended for multivariate damage states [43], and applied in a vibration modal analysis [46]. The basic idea of smooth orthogonal decomposition is to look for linear projections of matrix Y, which maximize both the overall smoothness of projection in time and its total variation. Mathematically, this translates into a generalized eigenvalue problem:

$$[Y^T Y]\psi = \lambda[(DY)^T DY]\psi\,, \tag{10}$$

where D is a discrete differential operator that can be approximated by a $(M-1) \times M$ matrix

$$D = \begin{bmatrix} -1 & 1 & 0 & 0 & \cdots & 0 \\ 0 & -1 & 1 & 0 & \cdots & 0 \\ \vdots & \ddots & \ddots & \ddots & \ddots & \vdots \\ 0 & \cdots & 0 & -1 & 1 & 0 \\ 0 & \cdots & 0 & 0 & -1 & 1 \end{bmatrix}. \tag{11}$$

The solution to Eq. (10) is usually obtained using *generalized singular value decomposition* of the matrix pair Y and DY, yielding:

$$\begin{aligned} Y &= UCX^T\,, \\ DY &= USX^T\,, \\ C^TC + S^TS &= I\,, \end{aligned} \tag{12}$$

where I is the identity matrix, the matrices U and V are unitary, X is a square matrix, and C and S are non-negative diagonal matrices. $\Psi = [\psi_1, \psi_2, \ldots, \psi_{N_e}] = X^{-T}$ is a matrix composed of eigenvectors, or *smooth orthogonal modes*. The columns of matrix UC contain *smooth orthogonal coordinates* (SOCs), and the corresponding eigenvectors or *smooth orthogonal values* (SOVs) are given by term-by-term division of $\mathrm{diag}(C^TC)^{1/2}/\mathrm{diag}(S^TS)^{1/2}$. The higher the value of SOV, the smoother in time is the corresponding SOC. Therefore, the dominant deterministic (i.e., *smooth*) trends in the feature space will correspond to the SOCs of the dominant SOVs. Therefore, the fatigue related trends are expected to be in SOCs with the largest SOVs.

2.3 Global and Local Fatigue Analysis

Fatigue first affects the muscle groups that work the hardest relative to their level of conditioning. As fatigue accumulates, movement kinematics are altered to relieve the fatigued muscles and load other muscle groups. Systemic fatigue in the body should reflect the amalgamation of the local fatigue processes that occur across all individual muscles involved in executing the task as well as changes in the central nervous system drive going to those muscles [20, 21, 22]. If there is no influx of new *external* energy (e.g., food, drinks or other nutritional energy sources) introduced into the system and if the workload is not altered, then it is assumed that the entire body will fatigue approximately monotonically (i.e., for constant power output and no energy input into the body the systemic fatigue is expected to accumulate monotonically). If new external energy were added, or if the external workload changed, then this systemic whole-body fatigue could easily be non-monotonic. However, in the present experiments, this was not the case and monotonic global systemic fatigue was expected.

Conversely, the *local* fatigue dynamics of *individual* muscles can go through cycles of both accumulation and relief if the movement kinematics are allowed to change and thus these local fatigue dynamics is expected to be *non-monotonic*. By analyzing movement kinematics data as described in the previous sections, it was expected that *global* fatigue trend would be captured by the dominant SOC. Lower order SOCs were expected to reflect *local* fatigue dynamics, which was estimated for individual muscles using standard EMG analysis (e.g., mean and median frequency trends from EMG power spectra). The minimum number of SOCs that were sufficient to accurately describe all local muscle activity as measured by mean and median frequencies was expected to provide reconstruction of the fatigue trajectory.

To show that local muscle fatigue information was embedded into the dominant SOCs, mean and median frequency curves were compared with the best affine (linear) projections of the SOCs onto those same curves. These projections were obtained by identifying linear combinations of SOCs that best fit the mean or median frequency curves in the least squares sense. To indicate how well the projection matched the local trends, R^2 values were calculated between them.

3 Experimental Design and Data Analysis

Seven highly trained (US Cycling Federation Category 3 or higher level of competition) male cyclists (Table 1) with no musculoskeletal or neurological deficits, participated after providing written informed consent. First, each subject completed a $\dot{V}O_{2\,\mathrm{max}}$ test using open-circuit spirometry during a graded exercise protocol. Approximately one week later, each subject returned to the lab to complete the actual fatigue trial. During this trial, each subject cycled on a Lode Excalibur Sport bicycle ergometer (Lode Medical Technology, Groningen, The Netherlands) at 100% of their $\dot{V}O_{2\,\mathrm{max}}$, until voluntary exhaustion [25], based on the protocol used in Refs. [18, 19]. Subjects were given vigorous verbal encouragement throughout the trials. Participants

Table 1: Basic characteristics for age (yrs), body mass (kg), years of training (yrs), $\dot{V}O_{2\,\mathrm{max}}$ (mL/kg/min), and time to fatigue (min:sec) for each cyclist.

Subject #	Age	Body Mass	Years of Training	$\dot{V}O_{2\,\mathrm{max}}$	Time to Fatigue
1	41	76.5	16	55.43	4:58
2	25	74.1	10	64.80	8:03
3	35	82.6	10	58.30	7:15
4	32	83.4	8	63.47	9:36
5	25	71.1	11	63.02	5:23
6	18	68.4	6	64.42	5:08
7	35	70.1	6	59.60	5:30
Mean±SD:	30.1 ± 7.8	75.2 ± 6.0	9.6 ± 3.6	61.3 ± 3.6	6:33 ± 1:46
Range:	18 – 41	68.4 – 83.4	6 – 16	55.4 – 64.8	4:58 – 9:36

were instructed to maintain 90 revolutions per minute (RPM) and were allowed to recover if their RPM fell below 90. Trials were terminated when cadence dropped below 70 RPM or when the subject felt they could no longer continue. Because all participants were highly trained competitive athletes, it is unlikely these subjects gave sub-maximal effort and/or terminated participation prematurely. Nevertheless, there could still have been psychological variations in motivation between subjects. Thus, we could not experimentally guarantee that all subjects had reached precisely the same fatigue state at the termination of their trial. Additional details of the experimental design are given in [25].

Each subject was marked with reflective markers to record sagittal plane kinematics for the trunk, hip, knee, and ankle angles of the left leg. Kinematic data were sampled at 120 Hz continuously throughout each trial using an 8-camera Vicon Motion Analysis system (Oxford Metrics, Oxford, UK). Raw marker data were first filtered through a low-pass filter with a cutoff frequency of 15 Hz.[4] Movement Kinematics were then calculated from the filtered marker data for the left side of the body [25].

Bipolar surface EMG electrodes (DE-2.1, Delsys Inc., Boston, MA, USA) were placed on the left leg over Biceps Femoris, Vastus Lateralis, Gastrocnemius, and the Tibialis Anterior muscles, according to accepted recommendations [48]. Although the Tibialis Anterior is not one of the major power producing muscles used during cycling, it was included in the present study to determine if the tracking methods adopted in the present study would still work for other muscles that play a supporting role in cycling. For example, while the Tibialis Anterior contributes only a small percentage of the power to the crank, this smaller muscle could still sustain significant fatigue [25] which could in turn affect how cyclists change their coordination strategies. EMG data for all muscles were sampled at 1080 Hz throughout the entire trial and were synchronized with the kinematic data. The raw EMG signals were first filtered through a digital bandpass filter with corner frequencies $\omega_1 = 30\,\mathrm{Hz}$ and $\omega_2 = 400\,\mathrm{Hz}$ to eliminate DC offset and aliasing. These EMG time series were then filtered through a digital notch filter with corner frequencies $\omega_1 = 59\,\mathrm{Hz}$ and $\omega_2 = 61\,\mathrm{Hz}$, as recommended in Ref. [49]. This was done to attenuate the small amounts of 60 Hz AC interference observed in the raw EMG signals, which was probably due to the electronics of the Lode Excalibur bicycle itself and/or other electronic devices in the lab at the time.

The recorded movement kinematics data were analyzed using both SSM-based and PSW-based features. Furthermore, complete feature sets, including both linear and nonlinear components, were compared to reduced feature sets containing only linear model based features. These comparisons allowed us to determine the importance of including nonlinear statistics in these analyses. The size of the data sets varied from subject-to-subject due to different lengths of time of cycling (approx. 5–10 min.). Therefore, for computing PSW-based features, each kinematic time series was partitioned into 60 disjoint windows of equal length and the PSW-based features were analyzed within each window. Construction of the SSM-based features required calculation of *long-time* statistical measures, which required longer time series. For these analyses, each kinematic time series was first partitioned into 30 disjoint windows of equal length. The variance of the estimated long-time measures scales as $1/\sqrt{N}$, where N in the number of points used in estimation. Using

[4]It is often recommended not to filter nonlinear time series using linear filters. However, in our case the cut-off frequency was set well beyond the observed bandwidth to eliminate aliasing.

30 windows provided a sufficient number of data points in each window to calculate long-time statistics with approximately the same variance as the short-time metrics computed using 60 windows. This reflects the fact that the short-time (PSW) metrics are better suited for short time series and if we had less data available, the long-time (SSM) analysis might not have been possible. To enable direct comparisons between SSM-based features and PSW-based features, the PSW analyses were repeated using 30 disjoint windows.

The goal of these kinematic analyses was to determine if these features, extracted *only* from the kinematic data, contained information regarding the systemic and local fatigue dynamics of cycling. To obtain *direct* measures of localized muscle fatigue for each EMG time series that were *independent* of the SSM- and PSW-based features extracted from the kinematics, both mean and median frequencies were calculated from each EMG signal. Mean and median frequencies were computed for each EMG signal for each down stroke and each up stroke of the pedals and then averaged to yield a single mean and median frequency value for each crank revolution. The resulting mean and median frequency time series were then box-car filtered, twice, with a moving window length of 9 frames to further smooth the mean and median frequency data. This "short-time Fourier transform" method was previously validated for tracking slowly varying changes in muscle fatigue across multiple dynamic contractions [28, 29, 30]. Other potential biomarkers of fatigue, such as cortisol levels and/or lactic acid accumulation, were not considered here since they are not traceable to individual muscles and could not be obtained continuously throughout each trial.

Finally, to compute direct correlations with the PSW-based tracking features, these smoothed mean and median frequency time series were partitioned into 60 disjoint windows of equal length and a single average value of mean and median frequency was calculated for each window. Dynamic contractions can also lead to variations in EMG center frequency due to changing muscle length [50]. However, the decreases in EMG center frequency across time during a fatiguing dynamic activity are generally due to changes in factors *within* the muscle itself (e.g., decreases in conduction velocity, de-recruitment of fast-twitch motor units, etc.), rather than changes in muscle length. Thus, the changes in EMG center frequency observed in this study were presumed to be due to changes in muscle fatigue and not to changes in muscle length [28, 29, 30].

4 Results

Time to fatigue varied from approximately 5–10 min across subjects (Table 1). These time-to-fatigue results were also consistent with those obtained from two other recent studies using a very similar protocol in a similar population [18, 19]. Basic measures of body anthropometrics and training histories also varied considerably across subjects (Table 1). Of the variables listed in Table 1, only body mass was weakly correlated to time to fatigue ($r^2 = 0.526$), but this correlation did not quite reach statistical significance (p = 0.0652).

Despite these differences in time-to-fatigue, all subjects maintained both power output and cadence at approximately constant levels until the final 10% of the fatigue trial (Fig. 1A). The precipitous drop-off in both cadence and power output during the last ∼10% of each trial indicates that these athletes had indeed reached their physical limits.

All subjects exhibited substantial non-monotonic changes in their local muscle fatigue states (i.e., mean or median frequencies) during these trials (Fig. 1B). The individual fluctuation patterns varied between muscles and across subjects. However, the majority of all muscles examined exhibited muscle fatigue (i.e., decreasing mean and/or median frequency) that was *sustained* across the entire trial, as determined by findings of statistically significant negative slopes obtained from linear fits to these data (Fig. 1B). Moreover, all muscles in all subjects exhibited some evidence of at least transient fatigue (median frequency decline was followed by recovery) at some point during each trial.

Likewise, the joint kinematic patterns observed for each subject also exhibited substantial non-monotonic changes over time during these trials (Fig. 1B). These changes were particularly apparent for shift in trunk lean. Here again, the individual fluctuation patterns varied between joint angles and across subjects, indicating that each subject was continuously altering their movement coordination strategy to maintain performance in spite of progressing muscle fatigue. Additional detailed descriptions and analyses of these these non-monotonic EMG and kinematic trends are published in Ref. [25]. In particular, those previous

analyses demonstrated that the fluctuations in local muscle fatigue states were correlated, on average, with subsequent alterations of movement kinematics [25]. However, those analyses did not yield specific predictive models for individual subjects.

4.1 Linear Versus Nonlinear Features

The SSM-based feature vector was composed of both linear and nonlinear statistics. The nonlinear components, which included skewness, kurtosis, correlation sum and fractal dimension, were removed from the feature space and compared with the feature space containing both linear and nonlinear components (Fig. 2). The SOVs for both analyses were of approximately same magnitude. Corresponding SOCs also displayed similar smoothness. Note that in both examples, SOC_1 exhibits smooth monotonic change over time (Fig. 2, b and f) and that the mode shapes for the higher SOCs (SOC_2, SOC_3, etc.) become increasingly more complex. Thus, SOC_1 reflects the sustained and overall systemic fatigue dynamics, while the higher order SOCs likely capture local transient (i.e., muscular) fatigue dynamics. However, there were clear differences in the shapes of these SOCs, which could have resulted from including nonlinear components. On the other hand, this could just be a result of including more statistics, and similar differences might be observable if other different linear measures are included in the feature vector, which was not done in this paper.

The same comparisons were done for the PSW-based features, where the movement kinematics obtained from the joint angles were analyzed using linear model based features and compared with the nonlinear model results (see Sec. 2.1.2). In Fig. 3, representative results for the knee angle data of subject 2 and the hip angle data of subject 6 are presented (note: values for variables are listed as: subject 2(subject 6)). In the linear model, Eq. (7), the model order was $p = 9(134)$ and for phase space partition $l = 1(1)$ was used. For the nonlinear model, the embedding dimension was 4(4), the delay time was 25(30), and the phase space was partitioned into 20(20) hyper-cuboids (5 partitions in each dimension). The entire time series was divided into 60 disjoint windows of 970(1,144) samples each. Studying the SOVs (Fig. 3), it was apparent that the linear analysis showed only one dominant mode. On the other hand, the nonlinear analysis had three(four) dominant modes. Looking at corresponding SOCs, nonlinear coordinates are substantially smoother and do not exhibit local fluctuations (noise) observed in the corresponding linear coordinates. Therefore, nonlinear effects are substantial and cannot be ignored at least in the PSW-based analysis. As with the SSM-based analyses (Fig. 2),the SOC_1's for the PSW-based analyses also exhibited smooth monotonic changes over time (Fig. 3, b and f), reflecting the sustained and overall systemic fatigue dynamics. Likewise, the mode shapes for the higher order SOCs increased in complexity, likely reflecting the local transient fatigue dynamics.

4.2 SSM (Long-Time) Versus PSW (Short-Time) Features

The complete (linear+nonlinear features) SSM-based analyses were then directly compared to the complete PSW-based analyses (Fig. 4). The parameters used for the PSW analysis were the same as for results described in the previous section, except that all analyses were conducted using 30 disjoint windows to allow direct comparison with the SSM analysis results. In these comparisons, the PSW-based SOCs generally exhibited slightly smoother characteristics, as evidenced by the magnitude of the corresponding SOVs. However, general trends were very similar despite the more prominent local fluctuations in the SSM-based SOCs. While the importance of nonlinear metrics was not very clear in SSM-based analysis (Fig. 3), these new results demonstrate that the variabilities observed in Fig. 3 where not just the result of using more features, but were brought by the consideration of nonlinear features. Thus, nonlinearities are important in both SSM and PSW analyses, since they provide additional information absent in the purely linear analysis. These results also illustrate the power of the PSW-based analysis as compared to the SSM-based analysis, for which the importance of nonlinear features was not apparent.

4.3 Local Fatigue Trends Embedded Into Global Systemic Fatigue Manifold

The primary goal of the present study was to determine if the SOCs—identified using SSM- and PSW-based analysis of the kinematics data—carried the information about the local muscle fatigue processes occurring

in individual muscles—as determined by the mean and median frequencies from the EMG data analysis. The EMG frequencies for individual muscles generically varied nonmonotonically over time (Figs. 5–6 [25]). These shifts reflect that subjects varyingly altered their movement strategies to maintain overall task performance in the face of progressing muscle fatigue. In this study, the dominant kinematics SOCs were projected onto scaled mean and median frequency trends in the least squares sense. The sample of results for the median frequency are shown in Fig. 5 from the SSM- and PSW-based analysis using ankle angles of subject 2, and in Fig. 6 for hip angles of subject 6. For these results only four SOCs were used, and these figures show best-case-scenario for the SSM-based features. In all other cases, PSW-based features provided a much better fit to the local trends when using the same number of SOCs as shown in Figs. 5–6.

To determine if the trends observed in Fig. 5 and Fig. 6 were consistent across subjects, we computed linear least squares fits (R^2) between the SOCs computed from the kinematic data and the mean and median frequency curves obtained from each subject. Results of these analyses are shown for ankle angles in Fig. 7 for median frequency. For the mean frequency the results were similar and are not shown here to save space. Similar results for hip angles are shown in Fig. 8. Additionally, these analyses show how many SOCs need to be included before the R^2 values plateau. These findings tell us how many SOCs are required to adequately describe the local EMG trends.

Across all subjects and comparisons, the PSW-based SOCs consistently provided much better fits for nearly all comparisons, regardless of the number of SOCs included. The PSW-based SOC analyses were also much more consistent, exhibiting less between-subject variability. In addition, for all subjects, approximately 4 PSW-based SOCs were needed to fully recover mean frequency trends, and possibly even fewer for the median frequency trends. Conversely, a much larger number of SOCs were needed from the SSM-based analyses to achieve the same correlations (R^2). These results demonstrate that the slow-time changes in human muscle fatigue are also fully represented in the changes that occur in movement kinematics.

5 Discussion

Repetitive strain injuries are highly prevalent among competitive and recreational cyclists [10, 11, 12, 13, 14, 15]. One possibility is that these cyclists become more prone to developing these injuries because they adopt non-optimal motion kinematics in response to muscle fatigue (e.g., [8, 9, 25]). An alternative possibility is that cyclists develop these injuries because they do not adjust their kinematics properly in response to changes in muscle fatigue, but instead continually load the same tissues in the same way beyond their threshold capacity. However, our group recently demonstrated that changes in muscle fatigue state were directly correlated with, and slightly *preceded*, specific changes in cycling kinematics [25], thus demonstrating that cyclists do change their kinematics in direct response to changes in localized muscle fatigue states. The purpose of this paper was to determine if there was a direct link between the muscle fatigue dynamics and changes in the kinematics of motion. To date, such links have not been established in the cycling literature. In the present paper, methods originally developed for fatigue identification in mechanical systems were adopted to analyze human cycling motion dynamics and to relate the observed kinematic changes to the local muscle fatigue as measured by EMG mean and median frequencies. The results of this study show that these approaches could directly predict each subjects level of fatigue based solely on their movement kinematics. The monotonic trends shown in the first SOCs (Figs. 2, 3 and 4) followed the overall fatigue level exhibited by each subject. Furthermore, the projections of the dominant SOCs onto the EMG mean and median frequency results (Figs. 5–6 and Figs. 7–8) demonstrate that this approach also directly predicted the local muscle fatigue states of individual muscles from strictly kinematic data.

The representative results of detailed comparisons of linear and nonlinear features based analyses were presented in the Figs. 2–3. The SSM-based features (Fig. 2) showed some differences in the higher-order SOCs, which could not be definitely attributed to the new information provided by inclusion of nonlinear features. A more comprehensive analysis including more statistics in the SSM features could have provided a more definite answer to this question. However, these analyses were not necessary after observing the clear superiority of nonlinear PSW-based features over the equivalent linear features (Fig. 3). The PSW results showed three or four dominant eigenvalues for nonlinear features versus just one for the linear. Thus, nonlinear analysis was found to be essential for capturing additional (higher-order) information in

the kinematics time series. This was not at all surprising as this was likely a logical result of the nonlinear coupling in the system between multiple joints and muscles.

Comparison of nonlinear SSM-based and PSW-based results (Fig. 4) showed that both methods provided highly correlated dominant SOCs that were attributed to the monotonic overall fatigue accumulation in the whole body. Higher-order SOCs were less correlated and here PSW-based SOCs showed fewer local fluctuations as indicated by larger corresponding SOVs. All this illustrated the advantages of short-time features over the long-time features: (1) PSW-based features are not arbitrary—they are specifically designed to quantify slow-time changes caused by parameters drifts [36, 43]; (2) SSM-based features are prone to be contaminated by dynamic (bifurcation) noise while PSW-based features are not [34, 33]; and (3) there is no *a priori* way to determine the optimal set of SSM-based features. However, it should be mentioned that in some lucky cases SSM-based features are expected to work as well as PSW-based features and require a much less computational effort.

The main question of this study was to determine if information regarding *local muscle* fatigue could be identified from the SOCs derived from the *kinematics* data. While it seems logical that changes in muscle fatigue would cause people to alter their kinematics, there are also many reasons why this might not be the case. Shifts and/or changes in movements kinematics could alternatively be due to other factors (e.g., discomfort, pressure from the seat, pain, etc.) not directly related to changes in central fatigue or in peripheral fatigue at the muscle level. Additionally, each muscle includes dozens of motor units and there are dozens of muscles involved in accomplishing the considered cycling task, which is controlled by the central nervous system. All of this suggests a highly complex system operating across a wide range of both length and time scales. However, the results of linear projection of several SOCs down to local muscle fatigue trends (Figs. 5–6) showed fairly good matches across all subjects and all muscle groups if enough SOCs (about four for PSW features) were considered. This suggests that there exists some low-dimensional model that can be used to model systemic muscle fatigue dynamics for this particular task at least over slow-time scales[5]. To our knowledge, while many previous papers have *speculated* about such links, the present work is the first to directly *quantify* these links.

The finding that these SOCs do project so well onto the local muscle fatigue trends raises the question of exactly what kinematic information is being reflected onto these EMG frequency trends. To begin to get an idea of this, one could potentially look at the weightings of each SOC used in each projection. However, these weightings varied somewhat for each case (i.e., for each combination of joint angle and muscle for each subject). Likewise, the individual SOCs themselves are combinations of the joint angle states defined for each joint angle time series and so these also varied for different subjects and different joint angles. This makes comparing and interpreting the quantitative contributions of the different individual SOCs across projections, and especially across subjects, rather complicated. While a full exploration of this issue is beyond the scope of the present paper, the strength of the findings presented here suggests that doing these analyses will be an important aspect of future research.

To get a better idea about cross-subject variability and performance of different features a detailed R^2 analysis was conducted for all kinematics time series for all subjects (Figs. 7–8), where the quality of embedding local trends into global measures is evaluated by the means average value of R^2 of the fits and corresponding standard deviation across all ten subjects. These results clearly showed that the PSW-based features consistently outperformed SSM-based features by providing considerably higher mean and lower standard deviation values for all possible combinations. In particular, only for the nonlinear PSW-based SOCs were all of the local trends recovered with the R^2 value 0.8 or larger. While for the SSM-based analyses, the fits still remained very poor for many EMG frequency statistics even if large number of SOCs were included in the projections. By looking at all the R^2 results, it was possible to state that the four-dimensional SOC manifold provided good representation of all local fatigue dynamics with 0.8 or better R^2 values.

The analyses conducted in this paper showed that by analyzing fast-time kinematics time series using nonlinear PSW metrics and smooth orthogonal decomposition, one can identify low-dimensional slow-time fatigue manifolds that embedded all of the local muscle fatigue dynamics. Therefore, the direct one-to-one experimental link between the muscle fatigue accumulation and subtle changes in motion dynamics was definitively

[5]Recall that our analysis is looking at averaged measures of fast-time dynamics over intermediate time-scales to get to the slow-time dynamics of muscle fatigue.

established. The importance of this result is three-fold. First, it provides experimental evidence that the systemic muscle fatigue process for this cycling task can be modeled by a low-dimensional dynamical system (i.e., very complex, high dimensional first principles physics-based models may not be necessary). Second, the smooth orthogonal decomposition of nonlinear PSW metrics calculated from kinematics time series can be used to track and detect subtle changes in *physiological* fatigue state. Finally, these changes in local muscle fatigue states can be detected by analyzing *only* motion kinematics data. This demonstrates that slowly evolving physiological process like muscle fatigue, which themselves are often not easy to measure and track directly, can still be extrapolated from easily observable biomechanical data. These findings provide a foundation for the development of procedures for tracking the progression or development of physiological fatigue, and potentially can be extended for use in early identification or detection of repetitive strain injuries. These analytical approaches and results could also have broader potential impact for understanding the basic connections between muscle physiology and kinematics and/or for enhancing performance for competition, etc.

6 Conclusion

In this paper a general, dynamical systems based framework for relating physiological fatigue processes to changes in motion kinematics was presented. It was demonstrated that the local slow-time changes in muscle fatigue dynamics were fully represented in the low-dimensional manifold identified through the analysis of fast-time motion kinematics. Thus, a direct one-to-one connection of muscle fatigue accumulation to the changes in motion coordination were experimentally demonstrated.

Ten highly trained competitive cyclists showed non-monotonic changes in local muscle fatigue as measured by the EMG median frequency. However, multivariate analysis of kinematics time series showed the existence of one dominant monotonic trend in the feature space. This was attributed to the cumulative (i.e. global) systemic fatigue occurring in the whole body. Additional analyses showed that nonlinear PSW-based kinematics features identified a four-dimensional smooth manifold (through smooth orthogonal decomposition) that embedded all of the localized muscle fatigue dynamics that occurred in individual muscles.

This study also showed the necessity of nonlinear analysis for capturing all localized muscle fatigue dynamics. In addition, the superiority of short-time PSW-based features over long-time SSM-based features was demonstrated in the R^2 analysis of linear fits across all subjects. PSW-based features require more computational resources, but they are specifically tailored to capture slow-time changes in dynamics and are insensitive to sudden changes in fast-time dynamics (bifurcations). It is true that SSM-based features are easier to compute and that in some cases they can yield results that are as good as PSW-based results. However, there is no *a priori* way to establish an optimal set of SSM metrics for a particular application that will work for all subjects. In contrast, PSW metrics consistently provide optimal results for all subjects and potentially for a variety of tasks. PSW-based methods therefore have great potential for tracking a variety of very important slow-time scale, "hidden" (i.e., not easily directly observable) physiological processes (e.g., muscle fatigue or repetitive strain injury) from readily observable biomechanical measures.

Acknowledgments

This study was supported in part by the National Institute of Biomedical Imaging and Bioengineering Grant No. 1R21EB003425-01A1 and the National Science Foundation Grant No. 0237792.

References

[1] MacIntosh, B. R., and Rassier, D. E., 2002. "What is fatigue?". *Canadian Journal of Applied Physiology,* **27**, pp. 42–55.

[2] Côté, J. N., Mathieu, P. A., Levin, M. F., and Feldman, A. G., 2002. "Movement reorganization to compensate for fatigue during sawing". *Experimental Brain Research,* **146**(3), pp. 394–398.

[3] Ebaugh, D. D., McClure, P. W., and Karduna, A. R., 2006. "Effects of shoulder muscle fatigue caused by repetitive overhead activities on scapulothoracic and glenohumeral kinematics". *Journal of Electromyography and Kinesiology,* **16**(3), pp. 224–235.

[4] Madigan, M. L., and Pidcoe, P. E., 2003. "Changes in landing biomechanics during a fatiguing landing activity". *Journal of Electromyography and Kinesiology,* **13**(5), pp. 491–198.

[5] Mizrahi, J., Verbitsky, O., Isakov, E., and Daily, D., 2000. "Effect of fatigue on leg kinematics and impact acceleration in long distance running". *Human Movement Science,* **19**(2), pp. 139–151.

[6] Sparto, P., Parnianpour, M., Reinsel, T., and Simon, S., 1997. "The effect of fatigue on multijoint kinematics, coordination, and postural stability during a repetitive lifting test". *Journal of Orthopaedic & Sports Physical Therapy,* **25**(1), pp. 3–12.

[7] Voge, K., and Dingwell, J., 2003. "Relative timing of changes in muscle fatigue and movement coordination during a repetitive one-hand lifting task". In *Proceedings of the 25th Annual International Conference of the IEEE Engineering in Medicine and Biology Society.* Institute of Electrical and Electronics Engineers, Cancun, Mexico, pp. 1807–1810.

[8] Rodgers, M. M., McQuade, K. J., Rasch, E. K., Keyser, R. E., and Finley, M. A., 2003. "Upper-limb fatigue-related joint power shifts in experienced wheelchair users and nonwheelchair users". *Journal of Rehabilitation Research and Development,* **40**(1), pp. 27–37.

[9] Sparto, P., Parnianpour, M., Reinsel, T., and Simon, S., 1997. "The effect of fatigue on multijoint kinematics and load sharing during a repetitive lifting test". *Spine,* **22**(22), pp. 2647–2654.

[10] Asplund, C., and Pierre, P. S., 2004. "Knee pain and bicycling". *Phys. Sports Med.,* **32**.

[11] Conti-Wyneken, A., 1999. "Bicycle injuries". *Phys. Meds Rehabil. Clin. N. Am.,* **10**, pp. 67–76.

[12] J. Holmes, A. L. P., and Whalen, N. J., 1994. "Lower extremity overuse in bicycling". *Clin. Sports Med.,* **13**, pp. 187–205.

[13] Dannenberg, A., Needle, S., Mullady, D., and Kolodner, K., 1996. "Predictors of injury among 1638 riders in a recreational long-distance bicycle tour: Cycle across maryland". *Am. J. Sports Med.,* **24**, pp. 747–753.

[14] Wilber, C., Holland, G., Madison, R., and Loy, S., 1995. "An epidemiological analysis of overuse injuries among recreational cyclists". *International Journal of Sports Medicine,* **16**, pp. 201–206.

[15] Dettori, N., and Norvell, D., 2006. "Non-traumatic bicycle injuries: a review of the literature". *Sports Medicine,* **36**, pp. 7–18.

[16] Abbiss, C. R., and Laursen, P. B., 2005. "Models to explain fatigue during prolonged endurance cycling". *Sports Medicine,* **35**(10), pp. 865–898.

[17] Millet, G. Y., and Lepers, R., 2004. "Alterations of neuromuscular function after prolonged running, cycling and skiing exercises". *Sports Medicine,* **34**(2), pp. 105–116.

[18] Gonzalez-Alonso, J., and Calbet, J. A. L., 2003. "Reductions in systemic and skeletal muscle blood flow and oxygen delivery limit maximal aerobic capacity in humans". *Circulation,* **107**(6), pp. 824–830.

[19] Mortensen, S. P., Dawson, E. A., Yoshiga, C. C., Dalsgaard, M. K., Damsgaard, R., Secher, N. H., and Gonzalez-Alonso, J., 2005. "Limitations to systemic and locomotor limb muscle oxygen delivery and uptake during maximal exercise in humans". *J Physiol,* **566**(1), pp. 273–285.

[20] Lepers, R., Hausswirth, C., Maffiuletti, N., Brisswalter, J., and van Hoecke, J., 2000. "Evidence of neuromuscular fatigue after prolonged cycling exercise". *Med Sci Sports Exerc,* **32**(11), pp. 1880–1886.

[21] Lepers, R., Maffiuletti, N. A., Rochette, L., Brugniaux, J., and Millet, G. Y., 2002. "Neuromuscular fatigue during a long-duration cycling exercise". *J Appl Physiol,* **92**(4), pp. 1487–1493.

[22] Sarre, G., Lepers, R., and van Hoecke, J., 2005. "Stability of pedalling mechanics during a prolonged cycling exercise performed at different cadences". *Journal of Sports Sciences,* **23**(7), pp. 693–701.

[23] Neptune, R., and Hull, M., 1999. "A theoretical analysis of preferred pedaling rate selection in endurance cycling". *Journal of Biomechanics,* **32**(4), pp. 409–415.

[24] Prilutsky, B. I., and Gregor, R. J., 2000. "Analysis of muscle coordination strategies in cycling". *IEEE Transactions on Rehabilitation Engineering,* **8**(3), pp. 362–370.

[25] Dingwell, J. B., Joubert, J. E., Diefenthaeler, F., and Trinity, J. D., In press. "Changes in muscle activity and kinematics of highly trained cyclists during fatigue". *IEEE Transactions on Biomedical Engineering*. Published Online: 2008-06-10, (doi: 10.1109/TBME.2008.2001130).

[26] DeLuca, C., 1984. "Myoelectrical manifestations of localized muscular fatigue in humans". *Critical Reviews in Biomedical Engineering,* **11**(4), pp. 251–279.

[27] Oka, H., 1996. "Estimation of muscle fatigue by using emg and muscle stiffness". In Engineering in Medicine and Biology Society. Bridging Disciplines for Biomedicine. Proceedings of the 18th Annual International Conference of the IEEE, Vol. 4, IEEE, pp. 1449–1450.

[28] MacIsaac, D., Parker, P., and Scott, R., 2001. "The short-time fourier transform and muscle fatigue assessment in dynamic contractions". *Journal of Electromyography and Kinesiology,* **11**(6), pp. 439–449.

[29] Beck, T. W., Housh, T. J., Johnson, G. O., Weir, J. P., Cramer, J. T., Coburn, J. W., and Malek, M. H., 2005. "Comparison of fourier and wavelet transform procedures for examining the mechanomyographic and electromyographic frequency domain responses during fatiguing isokinetic muscle actions of the biceps brachii". *Journal of Electromyography and Kinesiology,* **15**(2), pp. 190–199.

[30] Clancy, E. A., Farina, D., and Merletti, R., 2005. "Cross-comparison of time- and frequency-domain methods for monitoring the myoelectric signal during a cyclic, force-varying, fatiguing hand-grip task". *Journal of Electromyography and Kinesiology,* **15**(3), pp. 256–265.

[31] Doebling, A. W., Farrar, C. R., Prime, M. B., and Shevitz, D. W., 1996. Damage identification and health monitoring of structural and mechanical systems from changes in their vibration characteristics: A literature review. Tech. Rep. LA-13070-MS, Los Alamos National Laboratory, Los Almos, New Mexico 87545.

[32] Guttler, S., Kantz, H., and Olbrich, E., 2001. "Reconstruction of the parameter spaces of dynamical systems". *The American Physical Society,* **63**, p. 056215.

[33] Chelidze, D., and Liu, M., 2008. "Reconstructing slow-time dynamics from fast-time measurements". *Philosophical Transaction of the Royal Society A,* **366**, pp. 729–745.

[34] Chelidze, D., and Cusumano, J. P., 2006. "Phase space warping: nonlinear time series analysis for slowly drifting systems". *Philosophical Transactions of the Royal Society A,* **364**, pp. 2495–2513.

[35] Dingwell, J., Napolitano, D. F., and Chelidze, D., 2007. "A nonlinear approach to tracking slow-time-scale changes in movement kinematics". *Journal of Biomechanics,* **40**, pp. 1629–1634.

[36] Chelidze, D., Cusumano, J., and Chatterjee, A., 2002. "Dynamical systems approach to damage evalution tracking, part 1: desccription and experimental application". *Journal of Vibration and Acoutics,* **124**(2), pp. 250–257.

[37] Verdes, P., Granitto, P., Navone, H., and Ceccatto, H., 2001. "Nonstationary time-series analysis: accurate reconstruction of driving forces.". *Phys. Rev. Lett.,* **87**(12), p. 124101(4).

[38] Verdes, P., Granitto, P., and Ceccatto, H., 2006. "Overembedding method for modeling nonstationary systems". *Phys. Rev. Lett.,* **96**(11), p. 118701(4).

[39] Kantz, H., and Schreiber, S., 2004. *Nonlinear Time Series Analysis*, 2 ed.

[40] Bulmer, M., 1971. *Principles of Statistics*. Dover Publications.

[41] Carlos, S., 1998. "A procedure to estimate the fractal dimension of waveforms". *Complexity International,* **5**, pp. 17–42.

[42] January, G., and Zahra, M. "The fractality of lung sounds: A comparison of three waveform fractal dimension algorithms". *Chaos, Solitions, and Fractals,* **In Press**.

[43] Chelidze, D., 2004. "Identifying multidimensional damage in a hierarchical dynamical system". *Nonlinear Dynamics,* **31**, pp. 307–322.

[44] Chelidze, D., and Liu, M., 2006. "Multidimensional damage identification based on phase space warping: an experimental study". *Nonlinear Dynamics,* **46**, pp. 61–72.

[45] Sauer, T., Yorke, J. A., and Casdagli, M., 1991. "Embedology". *J. Stat. Phys.,* **65**(3–4), pp. 579–616.

[46] Chelidze, D., and Zhou, W., 2006. "Smooth orthogonal decomposition based modal analysis". *Journal of Sound and Vibration,* **292**(3–5), pp. 461–473.

[47] Chatterjee, A., Cusumano, J. P., and Chelidze, D., 2002. "Optimal tracking of parameter drift in a chaotic system: Experiment and theory". *Journal of Sound and Vibration.,* **250**(5), pp. 877–901.

[48] Konrad, P., 2005. *The ABC of EMG: A Practical Introduction to Kinesiological Electromyography*. Noraxon USA, Inc., Scottsdale, AZ.

[49] DeLuca, C., 1997. "The use of surface electromyography in biomechanics". *Journal of Applied Biomechanics,* **13**, pp. 135–163.

[50] Potvin, J., 1997. "Effects of muscle kinematics on surface emg amplitude and frequency during fatiguing dynamic contractions". *Journal of Applied Physiology,* **82**, pp. 144–151.

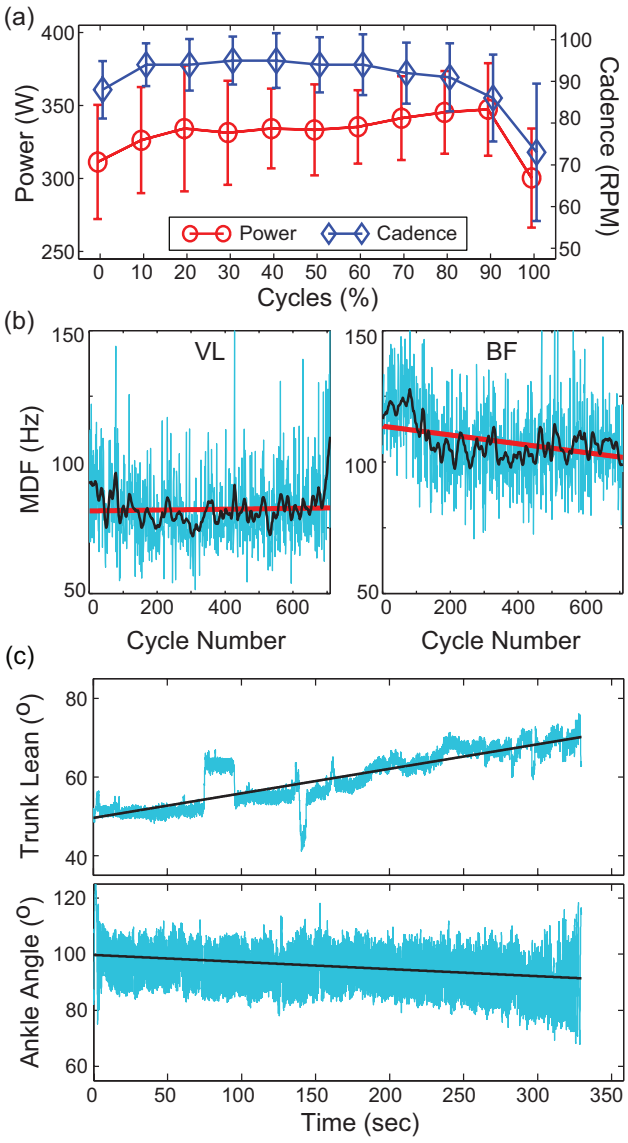

Figure 1: A) Average power output (Watts) and cadence (rev/min) as a function of the percentage of the trial completed for each subject. Symbols represent the average across subjects. Error bars represent between-subject standard deviations. B) Median frequency (MDF) results for the Vastus Lateralis (VL) and Biceps Femoris (BF) muscles for a typical subject. Thin lines show original averaged median frequency values. Thick black lines show the boxcar filtered median frequencies. The thick straight lines represent linear regression lines computed from the original median frequency data. C) Trunk Lean and Ankle angles for a typical subject. The thick straight lines represent linear regression lines.

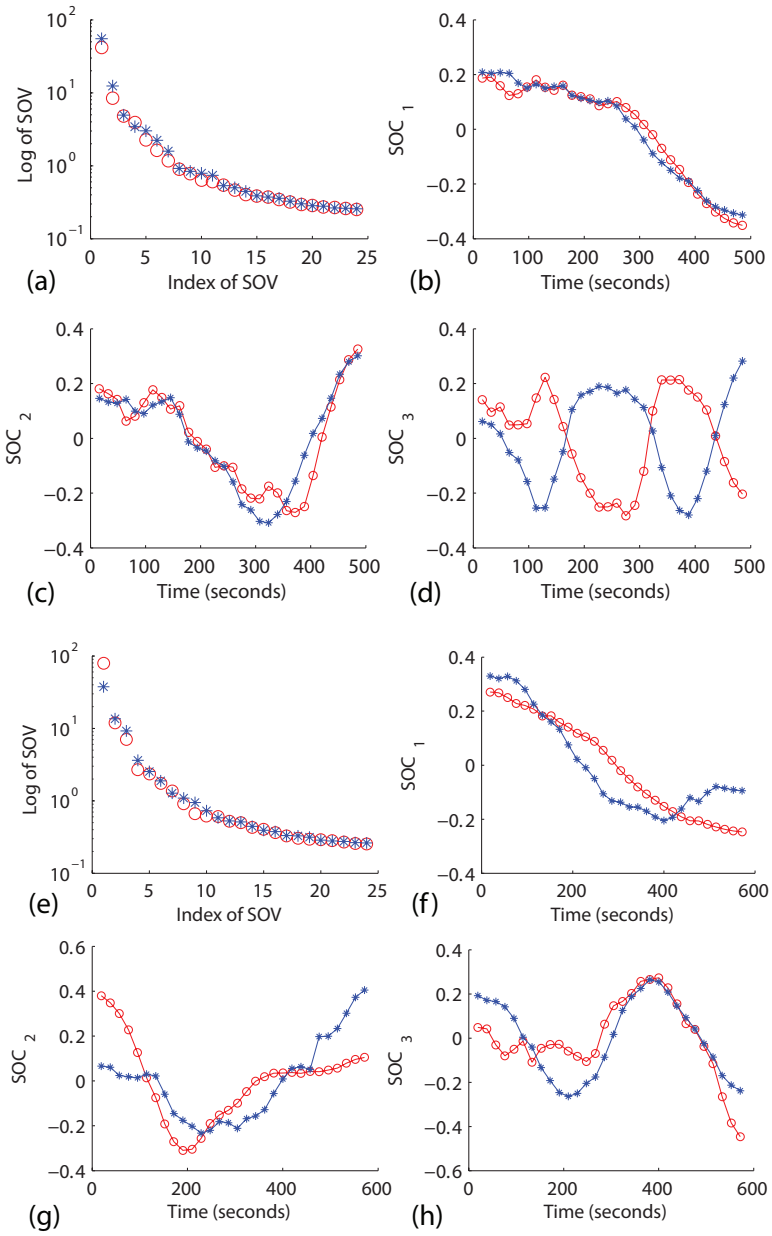

Figure 2: SSM-based multivariate analyses comparing combined linear+nonlinear (–∗–) vs. linear only (–○–) features for subject 2 ankle time series with $Y \in \mathbb{R}^{30\times 24}$ (a–d), and for subject 6 hip (e–h). Subplots (a) and (e) show the first 25 SOVs. No significant differences due to nonlinearity are observed. Subplots (b–d) and (f–h) show the corresponding first three SOCs, computed within 30 disjoint windows extracted from the original time series. Differences in these mode shapes could be due to the addition of the nonlinear components. Similar results were obtained from all other subjects and time series analyzed.

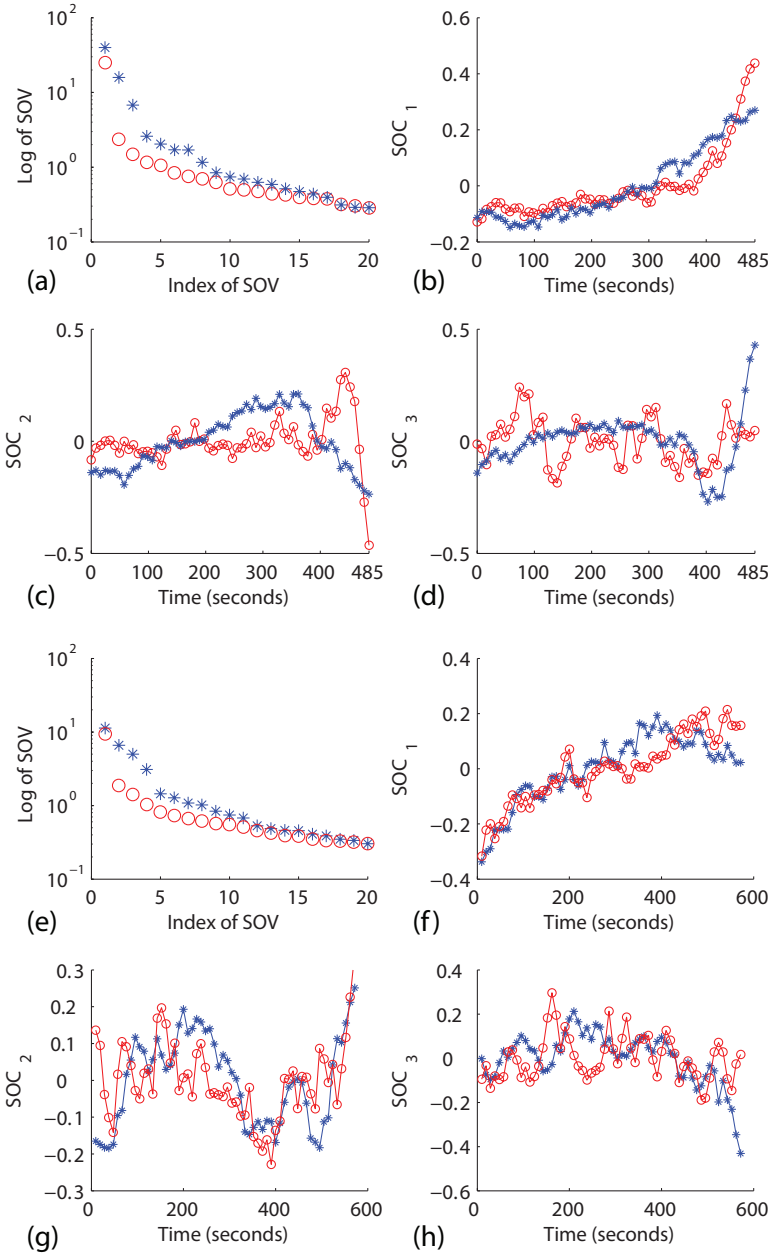

Figure 3: PSW-based multivariate analyses comparing combined linear+nonlinear (–∗–) vs. linear only (–○–) features for subject 2 ankle time series (a–d) and for subject 6 hip (e–h). Subplots (a) and (e) show the first 25 SOVs. Subplots (b–d) and (f–h) show corresponding first three SOCs, computed within 60 disjoint windows extracted from the original time series. While the linear features exhibited only one dominant SOC, adding the nonlinear features revealed three(four) dominant SOCs. These differences demonstrate that the linear only feature vectors were not sufficient to fully capture all of the relevant variations in these ankle time series. Similar results were obtained from all other subjects and time series analyzed.

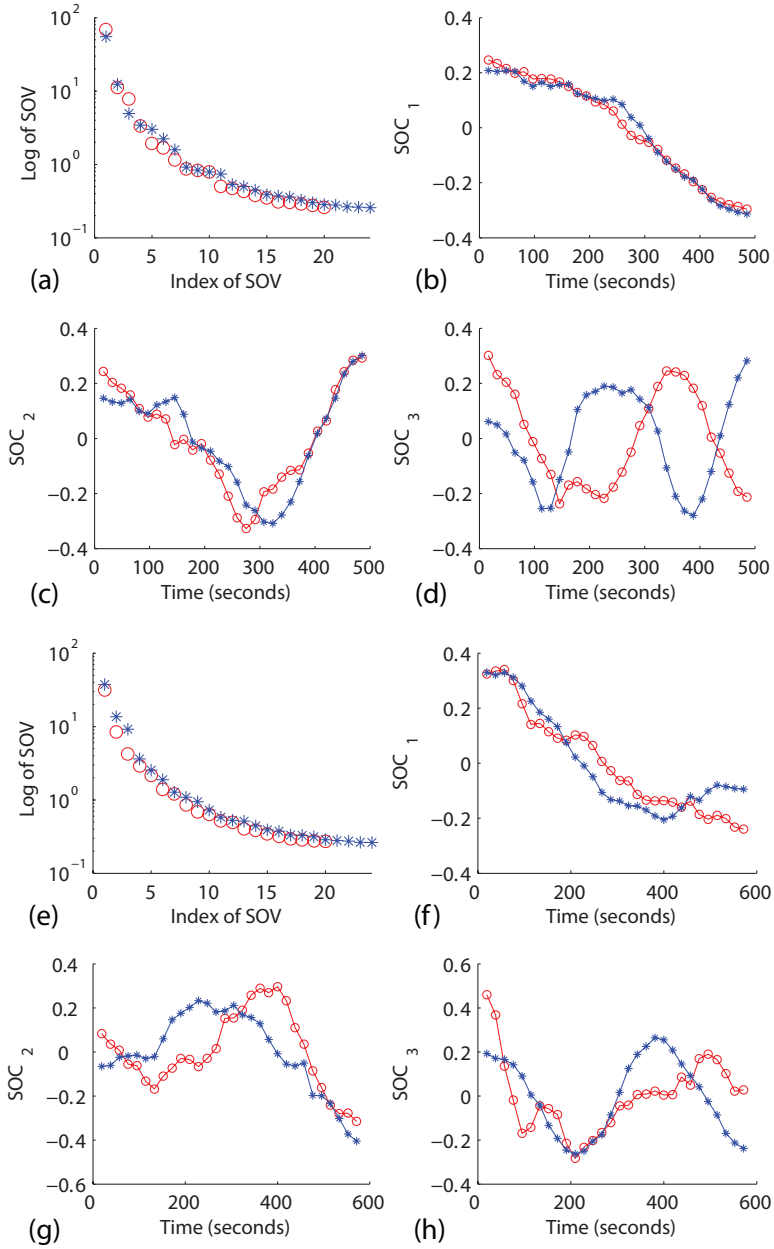

Figure 4: SSM-based (–∗–) and PSW-based (–○–) multivariate analysis for subject 2 ankle time series with $Y \in \mathbb{R}^{30\times 24}$ and $\mathbb{R}^{30\times 20}$, respectively (a–d), and for subject 6 hip (e–h). Subplots (a) and (e) show the first several SOVs, and subplots (b–d) and (f–h) show corresponding first three SOCs, computed within 30 disjoint windows extracted from the original time series. Similar results were obtained from all other subjects and time series analyzed.

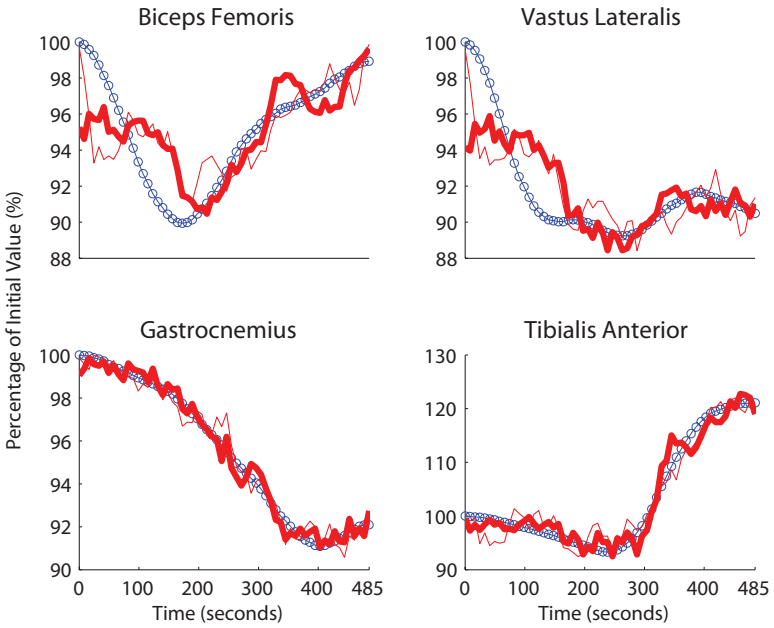

Figure 5: Projections of four SSM-based (thin solid lines) and PSW-based (thick solid lines) SOCs for subject 2 ankle angles onto EMG median frequency (–○–). Similar results were obtained from all other subjects and time series analyzed and for tracking both mean and median frequency trends. Both methods generally capture the local muscular trends. However, in all cases PSW-based SOCs provided generically better fits for the same number of SOCs used.

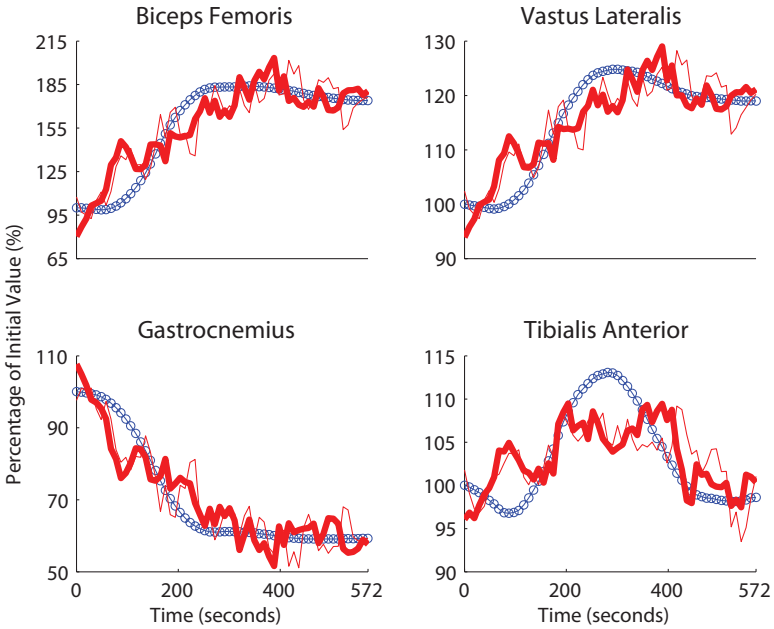

Figure 6: Projections of four SSM-based (thin solid lines) and PSW-based (thick solid lines) SOCs for subject 6 hip angles onto EMG median frequency (–○–). Similar results were obtained from all other subjects and time series analyzed and for tracking both mean and median frequency trends. Both methods generally capture the local muscular trends. However, in all cases PSW-based SOCs provided generically better fits for the same number of SOCs used.

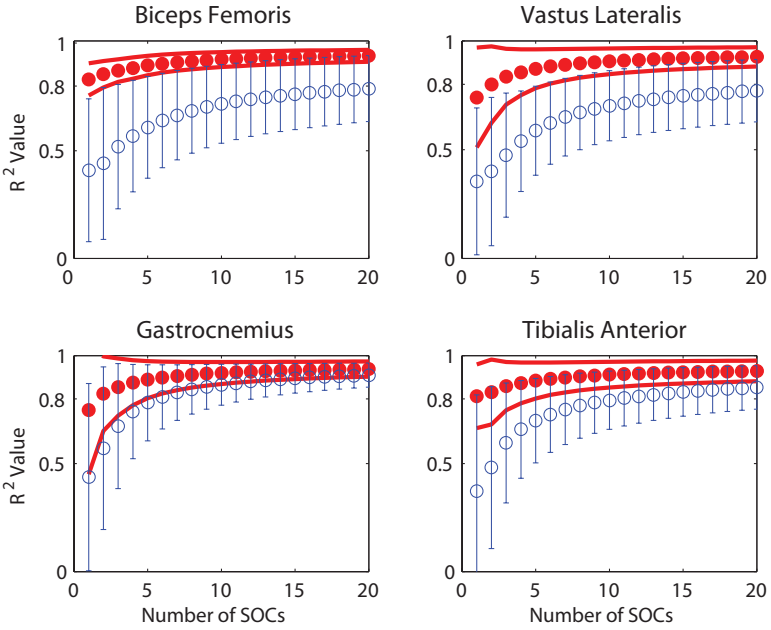

Figure 7: R^2 mean and standard deviations for ankle angle SSM-based fits (○) and PSW-based fits (●) to EMG median frequency. Error bars are ± one standard deviation. The PSW-based fits consistently outperformed the SSM-based fits.

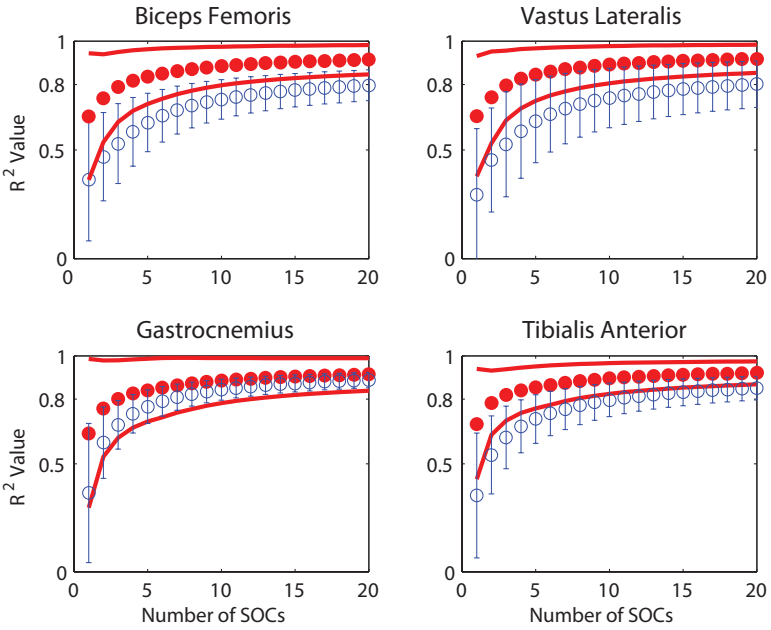

Figure 8: R^2 mean and standard deviations for hip angle SSM-based fits (○) and PSW-based fits (●) to EMG mean frequency. Error bars are ± one standard deviation. The PSW-based fits consistently outperformed the SSM-based fits.